PHYSICAL REVIEW D **84,** 015005 (2011)

Constraining selectron lightest supersymmetric particle scenarios with Tevatron trilepton searches

H. K. Dreiner*
Bethe Center for Theoretical Physics and Physikalisches Institut, Universität Bonn, Bonn, Germany

S. Grab†
SCIPP, University of California Santa Cruz, Santa Cruz, California 95064, USA

T. Stefaniak‡
Bethe Center for Theoretical Physics and Physikalisches Institut, Universität Bonn, Bonn, Germany
and II. Physikalisches Institut, Universität Göttingen, Göttingen, Germany
(Received 11 March 2011; published 6 July 2011)

The Tevatron collaborations have searched for associated production of charginos and neutralinos via trilepton final states. No events above the standard model prediction were observed. We employ these results to put stringent bounds on R-parity violating models with a right-handed scalar electron as the lightest supersymmetric particle. We work in the framework of lepton number violating minimal supergravity. We find that within these models, the complete parameter space consistent with the anomalous magnetic moment of the muon can be excluded at 90% confidence level. We also give prospects for Tevatron trilepton searches assuming an integrated luminosity of 10 fb^{-1}. We find that Tevatron will be able to test selectron lightest supersymmetric particle masses up to 170 GeV.

DOI: 10.1103/PhysRevD.84.015005 PACS numbers: 14.80.Ly, 11.10.Hi, 12.60.Jv, 13.85.−t

I. INTRODUCTION

The LHC has been running for over a year and first searches for supersymmetry [1,2] have been published [3–7]. In order to know what can possibly be expected at the LHC with present and forthcoming data, it is important to know the bounds implied by existing Tevatron searches [8–10]. It is our purpose here to investigate the bounds from Tevatron trilepton searches [11–16] on a specific supersymmetric scenario.

When extending the standard model (SM) of particle physics to include supersymmetry and implementing the minimal particle content, the supersymmetric standard model has more than 200 new parameters. Most of these arise from the supersymmetry breaking sector [1,2]. In order to be able to perform phenomenological studies, usually simpler models are considered. We focus here on the baryon triality (B_3) mSUGRA model [17,18], where B_3 is theoretically well motivated as an anomaly-free discrete gauge symmetry [19]. It has only 6 new parameters at the grand unification (GUT) scale ($M_{\text{GUT}} = \mathcal{O}(10^{16}\ \text{GeV})$)

$$M_0, M_{1/2}, A_0, \tan\beta, \text{sgn}(\mu), \mathbf{\Lambda}. \tag{1}$$

Here, M_0, $M_{1/2}$, and A_0 are the universal scalar mass, the universal gaugino mass, and the universal trilinear scalar coupling, respectively. $\tan\beta$ denotes the ratio of the two Higgs vacuum expectation values, and $\text{sgn}(\mu)$ fixes the sign of the bilinear Higgs mass parameter μ. $\mathbf{\Lambda}$ is a lepton-number and R-parity violating parameter described below.

In B_3 mSUGRA, the superpotential is extended by the lepton number violating (LNV) terms [20],

$$W_{\text{LNV}} = \tfrac{1}{2}\lambda_{ijk} L_i L_j \bar{E}_k + \lambda'_{ijk} L_i Q_j \bar{D}_k + \kappa_i L_i H_2, \tag{2}$$

which are absent in the minimal supersymmetric standard model. Here, L_i, Q_i, H_2, $\bar{E}_i$, and $\bar{D}_i$ are the standard chiral superfields. i, j, k are generation indices. λ_{ijk} and λ'_{ijk} are dimensionless couplings. The κ_i are dimensionful parameters, which vanish in B_3 mSUGRA at M_{GUT} due to a redefinition of the lepton and Higgs superfields [17]. They are generated at lower scales via the renormalization group equations (RGEs), leading to interesting phenomenological consequences for neutrino masses [21,22].

In the B_3 mSUGRA model, we assume that exactly one of the 36 dimensionless couplings in Eq. (2) is nonzero and positive at the GUT scale. The parameter $\mathbf{\Lambda}$ in Eq. (1) refers to this choice, i.e.,

$$\mathbf{\Lambda} \in \{\lambda_{ijk}, \lambda'_{ijk}\}, \qquad i, j, k = 1, 2, 3. \tag{3}$$

Given one coupling at M_{GUT}, other couplings that violate only the same lepton number are generated at the weak scale, M_Z, through the RGEs [17,23–25].

An important feature of B_3 mSUGRA models is that the lightest supersymmetric particle (LSP) is no longer stable. It is therefore not restricted to be electrically and color neutral [26]. Any supersymmetric particle can be the LSP. LNV interactions can significantly alter the RGE running

*dreiner@th.physik.uni-bonn.de
†sgrab@scipp.ucsc.edu
‡tim@th.physik.uni-bonn.de

TABLE I. List of $L_iL_j\bar{E}_k$ couplings (first column) needed to generate a $\tilde{e}_R$- or $\tilde{\mu}_R$-LSP (second column). The third column gives the most recent experimental bounds [95% confidence level (C.L.)], taken from Ref. [30]. The bounds apply at $M_{\rm GUT}$.

$L_iL_j\bar{E}_k$	LSP candidate	2σ bound
λ_{121}, λ_{131}	$\tilde{e}_R$	$0.020 \times (M_{\tilde{e}_R}/100\ \text{GeV})$
λ_{231}	$\tilde{e}_R$	$0.033 \times (M_{\tilde{e}_R}/100\ \text{GeV})$
λ_{132}	$\tilde{\mu}_R$	$0.020 \times (M_{\tilde{\mu}_R}/100\ \text{GeV})$

of the sparticle masses such that we obtain new candidates for the LSP beyond the lightest neutralino, $\tilde{\chi}_1^0$, and lightest stau, $\tilde{\tau}_1$ [27,28]. We recently showed in detail in Ref. [29] that the interplay of a large magnitude of (negative) A_0 with a $L_iL_j\bar{E}_k$ coupling $\Lambda \gtrsim \mathcal{O}(10^{-2})$ can lead to a right-handed slepton LSP, $\tilde{\ell}_R$, of the first or second generation, i.e., to a selectron, $\tilde{e}_R$, or smuon, $\tilde{\mu}_R$, LSP. The respective $L_iL_j\bar{E}_k$ couplings are given in Table I with their most recent 2σ upper bounds [30] at $M_{\rm GUT}$.

We also showed in Ref. [29] that our $\tilde{\ell}_R$ LSP scenarios naturally lead to multilepton final states at hadron colliders. For example, consider squark, $\tilde{q}$, pair production

$$\tilde{q}\,\tilde{q} \to qq\tilde{\chi}_1^0\tilde{\chi}_1^0 \to qq\ell\ell\tilde{\ell}_R\tilde{\ell}_R, \tag{4}$$

where the squark decays into a quark, q, and the $\tilde{\chi}_1^0$. The $\tilde{\chi}_1^0$ decays into the $\tilde{\ell}_R$ LSP and a charged lepton ℓ of the same flavor. The $\tilde{\ell}_R$ LSP can then decay via the $L_iL_j\bar{E}_k$ operator, for example,

$$\tilde{\ell}_R \to \ell'\nu, \tag{5}$$

i.e., into another charged lepton ℓ' and a neutrino ν.

We found in Ref. [29] that the LHC can test large regions of the $\tilde{\ell}_R$ LSP parameter space even with first data. These promising results have motivated us to investigate the present bounds on our model from Tevatron trilepton searches [8–10]: this is the topic of this paper. To be specific, we will concentrate on selectron LSP scenarios, where λ_{231} is the dominant R-parity violating coupling at $M_{\rm GUT}$. Because of the weaker experimental bound on λ_{231}, cf. Table I, we can obtain a lighter sparticle mass spectrum resulting in larger cross sections for sparticle pair production at the Tevatron.

We find that the Tevatron rules out the $\tilde{e}_R$ LSP parameter space within B_3 mSUGRA, which is consistent with the anomalous magnetic moment of the muon within 2 standard deviations.[1] One should thus also consider going beyond B_3 mSUGRA. We extrapolate the existing Tevatron analysis to an integrated luminosity of 10 fb^{-1} and find that more statistics can highly improve the sensitivity for heavier models. We therefore hope to encourage the Tevatron collaborations to search for our models in their upcoming trilepton supersymmetry (SUSY) searches.

This paper is organized as follows. In Sec. II, we review the $\tilde{e}_R$ LSP parameter space relevant for our analysis and develop two benchmark scenarios for the Tevatron. We then apply in Sec. III the most recent D0 trilepton search [8] to the benchmark points and show the $\tilde{e}_R$ LSP parameter space excluded by the Tevatron. In Sec. IV, we give prospects for future Tevatron analyses. We conclude in Sec. V. The Appendix presents the sparticle masses and branching ratios for our benchmark models.

II. THE SELECTRON LSP IN R-PARITY VIOLATING MSUGRA

A. Selectron LSP parameter regions

The phenomenology and the typical parameter space of B_3 mSUGRA models with a $\tilde{e}_R$ or $\tilde{\mu}_R$ LSP was discussed in detail in Ref. [29]. We review here the parameter space relevant for this work. In Fig. 1, we show a typical B_3 mSUGRA parameter region with a $\tilde{e}_R$ LSP in the $M_{1/2} - M_0$ plane. We have chosen a fairly large negative value of $A_0 = -1250$ GeV in order to enhance the (negative) effect of λ_{231} on the RGE running of the $\tilde{e}_R$ mass. The other parameters are $\tan\beta = 5$, $\text{sgn}(\mu) = +$ as well as $\lambda_{231} = 0.045$ at the GUT scale. We can identify a $\tilde{e}_R$, a $\tilde{\tau}_1$, and a $\tilde{\chi}_1^0$ LSP region. The solid gray region at low values of $M_{1/2}$ and M_0 is excluded by the bound on the LNV coupling; cf. Table I. The green contour line indicates the lower value of the 2σ window (using pion spectral functions from e^+e^- data[2]) of the SUSY contribution to the anomalous magnetic moment of the muon [32],

$$11.9 \times 10^{-10} < \delta a_\mu^{\rm SUSY} < 47.1 \times 10^{-10}, \tag{6}$$

i.e., parameter points left of the green line lie within the 2σ window and thus give a significant SUSY contribution to a_μ. Furthermore, the entire displayed region fulfills the 2σ constraints on the branching ratios of the decay $b \to s\gamma$ [33],

$$3.03 \times 10^{-4} < \mathcal{B}(b \to s\gamma) < 4.07 \times 10^{-4}, \tag{7}$$

and the 95% C.L. upper limit on the flavor-changing-neutral-current decay $B_s^0 \to \mu^+\mu^-$ [34],

$$\mathcal{B}(B_s^0 \to \mu^+\mu^-) < 3.6 \times 10^{-8}. \tag{8}$$

We also consider the bounds from Higgs searches at LEP on the light Higgs mass [35]. We employ FEYNHIGGS2.7.4 [36] for the calculation of the Higgs mass, as well as its production and decay properties. The excluded supersymmetric parameter space provided by HIGGSBOUNDS2.1.0 [37] is indicated as the patterned region in Fig. 1. We use SOFTSUSY3.0.13 [38,39] to calculate the SUSY spectrum and the Higgs mass parameters, and employ MICROMEGAS2.2 [40] to calculate $\mathcal{B}(b \to s\gamma)$, $\mathcal{B}(B_s^0 \to \mu^+\mu^-)$, and $\delta a_\mu^{\rm SUSY}$.

[1] The respective B_3 mSUGRA parameter space with a $\tilde{\mu}_R$ LSP is already ruled out by the stronger bound on λ_{132}; cf. Table I.

[2] Note that the SM prediction of a_μ is consistent with observations if one uses spectral functions from τ data [31].

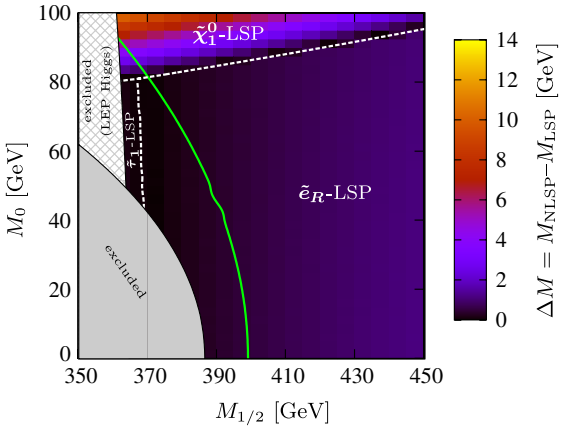

FIG. 1 (color online). Mass difference, ΔM, between the next-to LSP (NLSP) and LSP in the $M_{1/2} - M_0$ plane. The other B_3 mSUGRA parameters are $A_0 = -1250$ GeV, $\tan\beta = 5$, $\mathrm{sgn}(\mu) = +$, and $\lambda_{231}|_{\rm GUT} = 0.045$. The LSP candidate regions are shown, bordered by the white dotted lines. The solid gray region on the bottom left is excluded due to the bound on λ_{231}, cf. Table I, and the patterned region in the top left is excluded by Higgs searches at LEP. The green contour line indicates the SUSY contribution to the anomalous magnetic moment of the muon, $\delta a_\mu^{\rm SUSY}$. Models to the left lie within the 2σ window for $\delta a_\mu^{\rm SUSY}$; cf. Eq. (6).

In this study, we focus on light $\tilde{e}_R$ LSP models with an LSP mass $M_{\rm LSP} \lesssim 200$ GeV. A general feature of these scenarios is a near mass degeneracy[3] of the $\tilde{e}_R$ LSP with the lightest stau, $\tilde{\tau}_1$. Thus, a large portion of the $\tilde{e}_R$ LSP region exhibits a $\tilde{\tau}_1$ NLSP. However, close to the $\tilde{\chi}_1^0$ LSP region at larger values of M_0, we have $\tilde{e}_R$ LSP scenarios with $M_{\tilde{e}_R} \lesssim M_{\tilde{\chi}_1^0} \lesssim M_{\tilde{\tau}_1}$, i.e. a $\tilde{\chi}_1^0$ NLSP.

B. Benchmark scenarios for Tevatron searches

In this section, we select two benchmark scenarios which we test explicitly against the D0 trilepton analysis described in the next section. The B_3 mSUGRA parameters for the two benchmark points, denoted SUSY1 and SUSY2, are given in Table II. In both scenarios, the dominant R-parity violating coupling is $\lambda_{231} = 0.045$ at $M_{\rm GUT}$.

The benchmark point SUSY1 represents a wide region of the $\tilde{e}_R$ LSP parameter space, where the mass difference between the $\tilde{e}_R$ LSP and the lightest neutralino, $\tilde{\chi}_1^0$, is much larger than the mass difference between the $\tilde{e}_R$ LSP and the $\tilde{\tau}_1$ NLSP. The masses of the $\tilde{e}_R$, $\tilde{\tau}_1$, and $\tilde{\chi}_1^0$ are 139.1, 139.6, and 163.3 GeV, respectively. In fact, the next-to-NLSP (NNLSP) is the right-handed smuon, $\tilde{\mu}_R$, with a mass of 156.2 GeV. In contrast, SUSY2 lies in the boundary region

[3]A larger mass difference between $\tilde{e}_R$ and $\tilde{\tau}_1$ can be obtained by increasing Λ and/or $M_{1/2}$. However, larger values of Λ translate into the need for larger $\tilde{e}_R$ masses, *cf.* Table I. Thus, increasing either Λ or $M_{1/2}$ leads to heavier scenarios, which we do not consider here.

TABLE II. B_3 mSUGRA parameters for the benchmark points SUSY1 and SUSY2.

B_3 mSUGRA parameter	SUSY1	SUSY2
M_0 [GeV]	0	80
$M_{1/2}$ [GeV]	400	375
A_0 [GeV]	-1250	-1250
$\tan\beta$	5	5
$\mathrm{sgn}(\mu)$	$+$	$+$
$\lambda_{231}\|_{\rm GUT}$	0.045	0.045

to the $\tilde{\chi}_1^0$ LSP. Here, all three sparticles $\tilde{e}_R$, $\tilde{\tau}_1$, and $\tilde{\chi}_1^0$ are nearly degenerate in mass, with masses 151.5, 151.6, and 152.8 GeV, respectively. Because of the low mass difference between $\tilde{\chi}_1^0$ and $\tilde{e}_R$, we expect the electrons from the decay $\tilde{\chi}_1^0 \to \tilde{e}_R e$ to be fairly soft, such that many do not fulfill the preselection criteria [29]. Detailed tables containing all sparticle masses and decay modes for these benchmark models are given in the Appendix. Both SUSY1 and SUSY2 are chosen such that they are on the edge of the 2σ lower value of $\delta a_\mu^{\rm SUSY}$ (green line in Fig. 1).

III. CONSTRAINTS FROM THE TEVATRON

At the Tevatron at Fermilab, both experiments D0 [8] and CDF [9,10] have searched[4] for supersymmetry with final states containing three charged leptons, using the collected data of proton-antiproton ($p\bar{p}$) collisions at a center-of-mass energy $\sqrt{s} = 1.96$ TeV, corresponding to an integrated luminosity of 2.3 fb^{-1} and 3.2 fb^{-1}, respectively. These analyses were designed for the measurement of associated production of charginos and neutralinos [45] within R-parity conserving mSUGRA, using exclusive trilepton search channels [11–16]. Some of our lighter models could have led to an observable excess of events in these searches. Here we investigate quantitatively how these experimental analyses constrain the $\tilde{e}_R$ LSP parameter space.

We follow the D0 analysis to test the exclusion of $\tilde{e}_R$ LSP models. CDF uses a jet veto in the event selection, which is expected to lead to a reduced signal efficiency for many $\tilde{e}_R$ LSP models.[5] We therefore concentrate on the D0 search. Furthermore, D0 distinguishes their search channels by the flavor of the final state leptons. Since, in our models, the final state lepton flavor multiplicity depends on

[4]Note, that also other SUSY searches using the trilepton or (like-sign) dilepton signature have been performed at D0 and CDF [41–44]. At the current status, these analyses use at most a data set corresponding to 1.1 fb^{-1}. Thus, we do not expect these searches to be more restrictive than those presented here.

[5]In order to discriminate the $t\bar{t}$ background, CDF requires the scalar sum of the jet transverse energies $\sum E_T(\mathrm{jets}) \leq 80$ GeV and the number of jets $N(\mathrm{jets}) < 2$ [9]. We thus expect SUSY events from sparton (squark and/or gluino) pair production to be mostly rejected in the CDF analysis.

the choice of the Λ coupling, we expect different sensitivities of the D0 search channels for different choices of Λ.

In the next section, we describe how we emulate the D0 analysis and discuss the major changes to the original analysis. We test the two $\tilde{e}_R$ LSP benchmark points of Table II against our analysis in Sec. III B. We then review the results of the D0 analysis and show the excluded regions of the $\tilde{e}_R$ LSP parameter space.

A. The D0 trilepton analysis

The D0 search for associated production of charginos and neutralinos with final states containing three charged leptons is presented in Ref. [8]. The analysis is based on $p\bar{p}$ collision data at a center-of-mass energy of $\sqrt{s} = 1.96$ TeV corresponding to an integrated luminosity of 2.3 fb^{-1}, with the exception of the analysis using identified hadronic τ lepton decays, which is based on 1 fb^{-1} of data. Four dedicated trilepton event selections were designed, distinguished by the lepton content in the final state, i.e., we have a $ee\ell$, $\mu\mu\ell$, $e\mu\ell$, and $\mu\tau$ selection without specification of the lepton charge. Here the third lepton ℓ corresponds to a reconstructed isolated track without using the D0 standard lepton identification criteria. The first three channels are separated into a low-p_T and a high-p_T selection, while the $\mu\tau$ channel contains a $\mu\tau\ell$ selection and a $\mu\tau\tau$ selection. In this study, we focus on the $ee\ell$, $\mu\mu\ell$, and $e\mu\ell$ channels. The $\mu\tau$ selection turned out to be insensitive to our models.

In our object reconstruction, we use cone isolation criteria for all leptons, where the cone radius $\Delta R = \sqrt{(\Delta\phi)^2 + (\Delta\eta)^2}$ is given by the distance in pseudorapidity η and azimuthal angle ϕ. Guided by the D0 object reconstruction, an electron (muon[6]) with pseudorapidity $|\eta| < 3.2$ ($|\eta| < 2.0$) is considered as isolated, if the scalar sum of the absolute value of the transverse momenta of all tracks in a cone of $\Delta R = 0.4$ does not exceed 2.5 GeV. We do not loosen the reconstruction criteria for the third lepton ℓ but demand it to be an isolated electron or muon. Jets are reconstructed with FASTJET2.4.1 [46,47] using the kt algorithm with $R = 0.4$ and must be within $|\eta| < 2.5$. In our Monte Carlo simulation, the missing transverse energy, $\not{E}_T$, is calculated as the sum over the transverse momenta of all invisible particles.

In the following, we describe the general features of the various steps in the event selection. The details are given in Table III and the specific values should be taken from this table. For a detailed description of the cuts and their effect on the SM background, we refer the reader again to Ref. [8].

First, each selection requires two identified leptons ($\ell = e$, μ) with certain minimum transverse momenta $p_T^{\ell_1}$, $p_T^{\ell_2}$ (I). If more then two leptons are identified that satisfy the p_T criteria, the two leptons with the highest p_T are considered. Next, constraints on the invariant mass $m_{\ell_1\ell_2}$ and the opening angle $\Delta\phi_{\ell_1\ell_2}$ of the two leptons are imposed (II). This is followed in step III by requirements on $\not{E}_T$, the minimal transverse mass $m_T^{\min} = \min(m_T^{\ell_1}, m_T^{\ell_2})$, where

$$m_T^{\ell} = \sqrt{2 p_T^{\ell} \not{E}_T [1 - \cos\Delta\phi(\ell, \not{E}_T)]}, \tag{9}$$

and H_T, which is the scalar sum of the p_T of all jets with $p_T > 15$ GeV. In this step, a further requirement on $\mathrm{Sig}(\not{E}_T)$ is performed in the original D0 analysis, where $\mathrm{Sig}(\not{E}_T)$ is defined for events with at least one jet as

$$\mathrm{Sig}(\not{E}_T) \equiv \frac{\not{E}_T}{\sqrt{\sum_{\text{jets}} \sigma^2(E_T^j || \not{E}_T)}}. \tag{10}$$

Here, $\sigma^2(E_T^j || \not{E}_T)$ is the jet energy resolution projected on the $\vec{\not{p}}_T$ direction, i.e., on the direction of the missing transverse momentum vector.[7] This cut rejects events with $\not{E}_T$ faked by poorly measured jets and thus significantly reduces the QCD background. In our approach, we do not apply this cut on $\mathrm{Sig}(\not{E}_T)$, since we do not have a measure of the jet energy resolution. However, since the missing transverse energy stems mostly from the neutrinos coming from the leptonically decaying $\tilde{e}_R$ LSP, the effect of this cut is expected to be small.

In step IV, we demand an additional third lepton with a softer p_T requirement. Further cuts on its transverse mass $m_T^{\ell_3}$ and the invariant masses $m_{\ell_{1,2},\ell_3}$ of the third lepton with one of the preselected leptons are applied (V). For some channels in the original D0 analysis, step VI includes further lepton quality requirements using likelihood discriminants in order to reduce background from W boson production, where the second lepton is faked by jets or photons. This step is skipped in our approach, since this requires a more detailed simulation of the detector, beyond the scope of this work. In the last step (VII), we apply a cut on the product of the third lepton p_T and $\not{E}_T$ as well as on the p_T balance

$$p_T^{\text{bal}} = \frac{|\vec{p}_T^{\,\ell_1} + \vec{p}_T^{\,\ell_2} + \vec{\not{p}}_T|}{p_T^{\ell_3}}. \tag{11}$$

B. D0 Results and a test of two benchmark scenarios

In order to test whether our benchmark models are excluded, we have generated 2000 signal events, i.e., the pair production of all SUSY particles, scaled to an integrated luminosity of 2.3 fb^{-1} and apply the simplified D0 analysis described above. We employ the Feldman and Cousins method [48] to set 90% C.L. upper limits given the number of expected background events and the number of observed events, both taken from the D0 paper [8].

[6]This isolation criteria corresponds to *tight* muons in Ref. [8].

[7]Note that in Ref. [8] the symbol $\vec{\not{E}}_T$ is used.

TABLE III. D0 selection criteria for the $\mu\mu\ell$, $ee\ell$, and $e\mu\ell$ analyses for the low-p_T selection and the high-p_T selection; see text and Ref. [8] for further details. All energies, masses, and momenta are in GeV, angles are in radians. We apply all cuts except the cut on Sig($\not\!\!E_T$) in step III and the anti-W requirements in step VI.

	Selection	$\mu\mu\ell$		$ee\ell$		$e\mu\ell$	
		low p_T	high p_T	low p_T	high p_T	low p_T	high p_T
I	$p_T^{\ell_1}$, $p_T^{\ell_2}$	>12, >8	>18, >16	>12, >8	>20, >10	>12, >8[a]	>15, >15
	$m_{\ell_1\ell_2}$	$\in$ [20, 60]	$\in$ [0, 75]	$\in$ [18, 60]	$\in$ [0, 75]	...	...
II	$\Delta\phi_{\ell_1\ell_2}$	<2.9	<2.9	<2.9	<2.9	...	...
	$\not\!\!E_T$	>20	>20	>22	>20	>20	>20
	Sig($\not\!\!E_T$)	>8	>8	>8	>8	>8	>8
	$m_T^{\min}$	>20	>20	>20	>14	>20	>15
III	H_T	...	<80	...	...	...	...
IV	$p_T^{\ell_3}$	>5	>4	>4	>12	>6	>6
	$m_T^{\ell_3}$	>10	>10	>10	>10	>10	>8
V	$m_{\ell_{1,2}\ell_3}$	$\notin$ [80, 110]	...	...	...	<70	<70
VI	anti-W	...	...	tight likelihood[b]	...	tight likelihood[c] hit in 2 inner layers[c] very tight muon isolation[d] $\sum_{0.05<\Delta R<0.4} p_T^{\ell_3} < 1$	
	$E_T \times p_T^{\ell_3}$	>200	>300	>220	...	...	...
VII	p_T^{bal}	<4	<4	<4	<4	<2	<2

[a] $p_T^{\ell_1}$ and $p_T^{\ell_2}$ are electron and muon p_T, respectively.
[b] for $p_T^{\ell_3} < 15$ GeV
[c] for $m_T^{\mu} \in [40, 90]$ GeV
[d] for $m_T^{e} \in [40, 90]$ GeV

In those cases where the number of observed events is smaller than the expected background, we take as the upper limit the 90% C.L. *sensitivity*, defined as the average upper limit that would be obtained by an ensemble of experiments with the expected background and no true signal, and given in Table XII in Ref. [48].[8] We claim a 90% C.L. exclusion of the SUSY scenario, if the number of signal events exceeds this upper confidence limit in any step of the event selection. We do this comparison separately for all four[9] selection channels in order to gain some insight into their sensitivity to our models. Note that in this method, systematic uncertainties are not taken into account. For the calculation of the Feldman and Cousins confidence limits we employ ROOT [49].

For the simulation, we use SOFTSUSY3.0.13 [38,39] to calculate the SUSY mass spectra. The SOFTSUSY output is fed into ISAWIG1.200 and ISAJET7.64 [50] in order to calculate the decay widths of the SUSY particles including the relevant R-parity violating decays. We have also added some missing three-body slepton decays to the ISAJET code; see Ref. [29] for details. The signal process, i.e., sparticle pair production, was simulated with HERWIG6.510 [51–53].

For the two benchmark models, the leading-order (LO) cross sections of the following supersymmetric production processes are given in Table IV: sparton (i.e., squark and

TABLE IV. Leading-order signal cross sections for $p\bar{p}$ collisions at a center-of-mass energy of $\sqrt{s} = 1.96$ TeV for the benchmark scenarios SUSY1 and SUSY2. We give the cross section of sparton (i.e., squark and gluino) pair, slepton pair, and electroweak gaugino pair/EW gaugino-sparton production separately. The last row gives the total sparticle pair production cross section, which is the signal process. We employed HERWIG6.510 to derive the LO cross sections and for the event simulation. The uncertainties are due to statistical fluctuations from HERWIG.

Signal cross section (in fb)	SUSY1	SUSY2
$\sigma(p\bar{p} \to$ sparton pairs$)$	1.5 ± 0.1	8.3 ± 0.2
$\sigma(p\bar{p} \to$ slepton pairs$)$	8.5 ± 0.2	6.5 ± 0.1
$\sigma(p\bar{p} \to$ gaugino pairs, gaugino-sparton$)$	3.8 ± 0.1	6.1 ± 0.1
$\sigma(p\bar{p} \to$ sparticle pairs$)$	13.8 ± 0.2	20.9 ± 0.2

[8] For the number of expected background events >15, we approximate the sensitivity by the Feldman and Cousins upper limit for $N_{\text{obs}} = N_{\text{bkg}}$. This is only relevant for the extrapolation to 10 fb^{-1} in Sec. IV.

[9] As mentioned before, the fourth channel including τ leptons is insensitive. Thus we do not present the results for this specific channel here.

TABLE V. Numbers of events observed in the data and expected for the background (taken from Ref. [8]) and numbers of signal (SUSY1 and SUSY2, see text) events at various stages of the analysis for the $\mu\mu\ell$, $ee\ell$, and $e\mu\ell$ channels and the low-p_T selection. Each row corresponds to a group of cuts, as detailed in Table III. This is for an integrated luminosity of 2.3 fb^{-1}.

Selection	$\mu\mu\ell$				$ee\ell$				$e\mu\ell$			
	Data	Backgrd.	SUSY1	SUSY2	Data	Backgrd.	SUSY1	SUSY2	Data	Backgrd.	SUSY1	SUSY2
I	194 006	195 557 ± 177	6.6	17.8	235 474	232 736 ± 202	19.8	11.7	16 630	16 884 ± 75	12.6	18.2
II	22 766	26 067 ± 88	1.4	4.2	31 365	27 184 ± 64	4.8	2.8				
III	178	181 ± 6.4	1.2	3.9	515	212 ± 12	4.3	2.6	1191	1177 ± 20	11.1	16.9
IV	7	2.9 ± 0.7	1.0	2.8	16	9.3 ± 2.0	3.0	1.3	22	18.0 ± 1.2	9.9	11.0
V	4	2.2 ± 0.5	0.6	2.4	9	5.9 ± 1.7	2.8	1.3	3	3.5 ± 0.5	3.8	3.9
VI					6	3.1 ± 0.4			2	1.6 ± 0.4		
VII	4	1.2 ± 0.2	0.5	1.8	2	1.8 ± 0.2	2.4	1.2	2	0.8 ± 0.2	1.2	1.0

TABLE VI. Same as Table V, but for the high-p_T selection. Signal event yields that exceed the 90% C.L. upper exclusion bound are boldface.

Selection	$\mu\mu\ell$				$ee\ell$				$e\mu\ell$			
	Data	Backgrd.	SUSY1	SUSY2	Data	Backgrd.	SUSY1	SUSY2	Data	Backgrd.	SUSY1	SUSY2
I	140 417	141 781 ± 120	5.4	16.2	171 001	170197 ± 175	19.0	11.1	4617	4709 ± 23	10.6	17.0
II	10 349	10 645 ± 51	1.9	5.6	8273	7937 ± 39	6.8	3.9				
III	173	176 ± 5.7	1.2	3.7	244	264 ± 10	6.4	3.8	727	738 ± 11	9.8	16.0
VI	7	3.8 ± 0.5	0.9	2.8	0	1.5 ± 0.3	3.9	1.8	11	12.7 ± 0.9	**8.8**	**10.3**
V	4	2.9 ± 0.4	0.9	2.8	0	1.1 ± 0.3	3.7	1.8	2	2.8 ± 0.5	3.3	3.6
VI									0	1.0 ± 0.2		
VII	4	2.0 ± 0.3	0.9	2.4	0	0.8 ± 0.1	**3.4**	1.7	0	0.5 ± 0.1	0.9	1.0

gluino) pair production, slepton pair production, and electroweak (EW) gaugino pair, as well as, EW gaugino-sparton production. For the point SUSY1, sparticle production is dominated by slepton and gaugino production. In contrast, for SUSY2 the sparton production dominates due to the low mass of the lightest stop, $M_{\tilde{t}_1} = 304.9$ GeV, which decays exclusively to the lightest chargino and a bottom quark, cf. Table VIII.

Note that higher order corrections usually enhance SUSY and SM particle production at hadron colliders by several tens of percent [45,54,55]. Therefore, as a conservative approach, we only use the LO cross section for the signal, while the SM di-boson, Υ, $t\bar{t}$, and W + jet background in the D0 analysis [8] is normalized to the next-to-leading (NLO) cross section. The Drell-Yan background is even normalized to the next-to-NLO cross section and the multijet background is estimated directly from D0 data.[10] After all selection criteria are applied, the SM background is dominated by WZ production.

In Table V and VI, we review the results from the D0 analysis and compare them with the results for the two B_3 mSUGRA models SUSY1 and SUSY2 for the low-p_T and the high-p_T selections, respectively.

[10]Unfortunately, Ref. [8] gives no references for the NLO and next-to-NLO cross sections used in their analysis.

In all selections, the signal event yield for both benchmark scenarios is $\lesssim 20$ events after the two lepton requirement (step I) and for an integrated luminosity of 2.3 fb^{-1}. Thus, the event yields in the first steps (I–III) of the analysis are dominated by the overwhelming SM background. The analysis becomes sensitive to the signal once we require the third lepton (step IV and beyond). Then, the SM background is reduced to $\mathcal{O}(1$–$20)$ expected events. We now discuss in detail the D0 results and the signal event yields of the different selections after step IV of the analysis was performed.

In the $\mu\mu\ell$ channel (in both the low-p_T and high-p_T selection), the number of events observed by D0 is larger than the number of expected events from the SM background for all steps beyond cut IV. Therefore, this channel has intrinsically a less restrictive impact on the SUSY models. We expect only $\mathcal{O}(1$–$3)$ signal events beyond step IV for both benchmark points. Hence, the $\mu\mu\ell$ channel cannot exclude the SUSY1 and SUSY2 models.

Note that SUSY2 yields roughly 3 times as many events in this selection as SUSY1. This is due to the enhanced $\tilde{t}_1$ pair production and their decay to the lightest chargino, as mentioned above. The chargino decays to the $\tilde{\nu}_\mu$ and a muon 21% of the time, leading to an enhanced number of muons in the signal. However, in the $\mu\mu\ell$ high-p_T selection, most of the signal events from sparton-pair production are rejected by the H_T cut in step III. This reduces, in

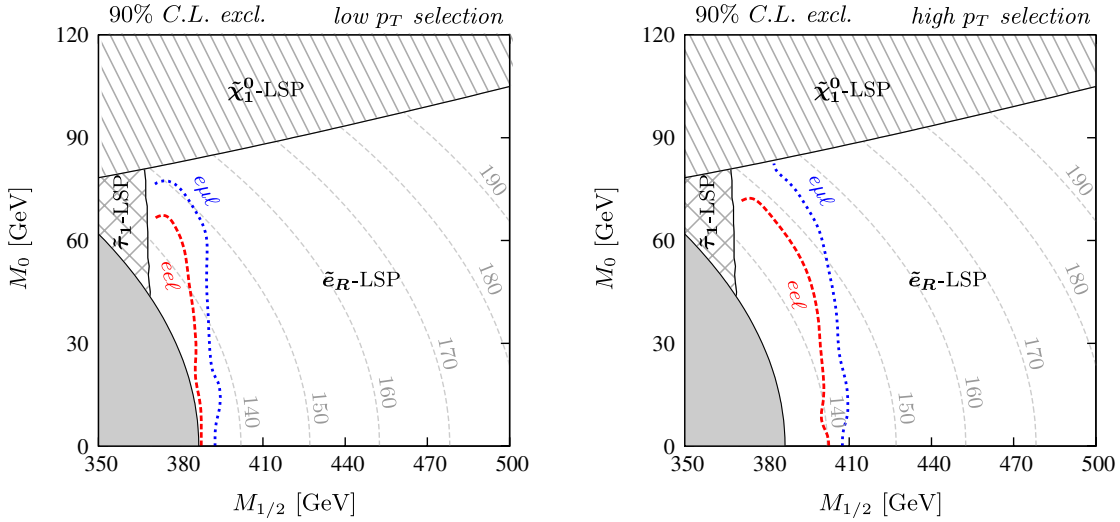

(a) Excluded $\tilde{e}_R$ LSP parameter space with the low-p_T selections.

(b) Excluded $\tilde{e}_R$ LSP parameter space with the high-p_T selections.

FIG. 2 (color online). Excluded regions (90% C.L.) of the $\tilde{e}_R$ LSP parameter space by the D0 trilepton analysis with 2.3 fb^{-1} of data. We choose $\lambda_{231} = 0.045$ as the dominant LNV coupling at $M_{\rm GUT}$. The other parameters are $A_0 = -1250$ GeV, $\tan\beta = 5$, and $\mathrm{sgn}(\mu) = +$. The colored contour lines give the excluded region by the different channels: In Fig. 2(a), they correspond to the $ee\ell$ (red, dashed line) and $e\mu\ell$ (blue, dotted line) low-p_T selections, while in Fig. 2(b) they are shown for the same channels in the high-p_T selection. The gray dotted contour lines give the LSP mass, $M_{\tilde{e}_R}$, in GeV, as indicated by the labels.

particular, the SUSY2 event yield, since here the production of sparton-pairs comprises 40% of the signal cross section, cf. Table IV.

In the $ee\ell$ channel, the number of observed events is larger (lower) than the number of expected SM background events in the low-p_T (high-p_T) selection for all steps beyond cut IV. For both benchmark scenarios, we expect $\mathcal{O}(1$–$4)$ signal events in these steps of the analysis. Furthermore, the number of expected signal events for SUSY1 is roughly 2 times more than for SUSY2. This is because in SUSY2, the mass difference between the $\tilde{\chi}_1^0$ and the $\tilde{e}_R$ LSP is small. Therefore, the electrons from the decay $\tilde{\chi}_1^0 \rightarrow \tilde{e}_R e$ tend to be soft and fail to pass the p_T criteria in step I of the $ee\ell$ selection. The SUSY1 event yield exceeds the 90% C.L. upper bound in step VII of the high-p_T $ee\ell$ selection and is therefore excluded by the D0 trilepton search.

For the low-p_T selection of the $e\mu\ell$ channel, the number of observed events tends to be larger than the number of expected SM background events, whereas in the high-p_T selection, the number of observed events is slightly less. Both the SUSY1 and SUSY2 event yield exceed the 90% C.L. upper limit in step IV of the $e\mu\ell$ high-p_T selection. The following steps in the $e\mu\ell$ channel (step V and beyond) are not as sensitive to our models as step IV, because the cut on the dilepton invariant masses in step V significantly reduces the signal.

In general, the B_3 mSUGRA parameter region close to a $\tilde{\chi}_1^0$ LSP is more difficult to exclude due to the soft electrons. For instance, in step IV of the $e\mu\ell$ low-p_T selection, the 90% C.L. upper limit is 13.0 events, while we expect 11.0 signal events for SUSY2. However, if we modify the M_0 value of SUSY2 from 80 GeV to 75 GeV, i.e., we basically change the mass difference between $\tilde{\chi}_1^0$ and $\tilde{e}_R$ from 1.3 to 3.7 GeV, the number of expected signal events increases to 15.2 events and the model is excluded.

We conclude, that the D0 analysis using 2.3 fb^{-1} of integrated luminosity excludes both benchmark points SUSY1 and SUSY2 at 90% C.L. The most restrictive channels for $\tilde{e}_R$ LSP models with a dominant λ_{231} coupling are the $ee\ell$ high-p_T selection (in step VII) and the $e\mu\ell$ high-p_T selection (in step IV). In the next section, we determine the excluded regions of the $\tilde{e}_R$ LSP parameter space.

C. Excluded selectron LSP parameter space

We now apply the D0 analysis to a more extensive $\tilde{e}_R$ LSP parameter region. For this, we perform a scan in the $M_{1/2} - M_0$ plane with $M_{1/2} \in [350\ \text{GeV}, 500\ \text{GeV}]$ in steps of $\Delta M_{1/2} = 5$ GeV and $M_0 \in [0\ \text{GeV}, 120\ \text{GeV}]$ in steps of $\Delta M_0 = 2.5$ GeV. We retain $\lambda_{231} = 0.045$ at $M_{\rm GUT}$. The other B_3 mSUGRA parameter values are $A_0 = -1250$ GeV, $\tan\beta = 5$, and $\mathrm{sgn}(\mu) = +$. The scanned $\tilde{e}_R$ LSP parameter region was already discussed in Sec. II A; cf. Fig. 1. For each parameter point with a $\tilde{e}_R$ LSP, 2000 signal events were generated and scaled to an integrated luminosity of 2.3 fb^{-1}. Then the $ee\ell$, $\mu\mu\ell$, and $e\mu\ell$ low-p_T and high-p_T event selections were applied[11]. At each step of the

[11]We did the same for the $\mu\tau$ selection for an integrated luminosity of 1.0 fb^{-1}. However, this channel is not capable of excluding any $\tilde{e}_R$ LSP parameter space. Thus, we do not show any results for the $\mu\tau$ channels.

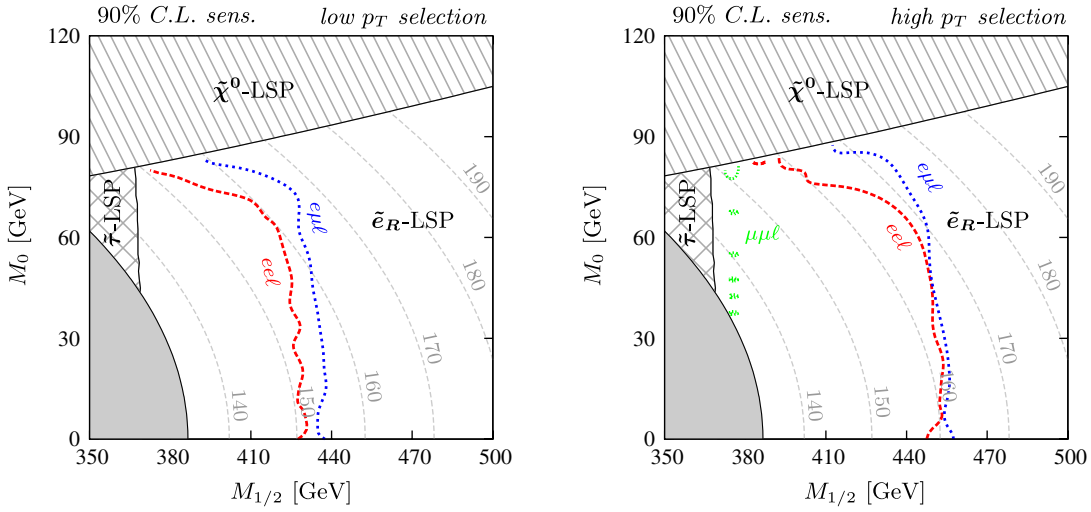

(a) $\tilde{e}_R$ LSP sensitivity region with the low-p_T selections. (b) $\tilde{e}_R$ LSP sensitivity region with the high-p_T selections.

FIG. 3 (color online). Extrapolated sensitivity regions (90% C.L.) of the $\tilde{e}_R$ LSP parameter space for the D0 trilepton analysis with future data corresponding to an integrated luminosity of 10 fb^{-1}. The parameter regions are the same as in Fig. 2. The colored contour lines give the sensitivity of the different channels: In Fig. 3(a), they correspond to the $ee\ell$ (red, dashed line) and $e\mu\ell$ (blue, dotted line) low-p_T selections, while in Fig. 3(b) they are shown for the same channels in the high-p_T selection. Furthermore, the fine dotted, green contour line in Fig. 3(b) gives the sensitivity of the $\mu\mu\ell$ high-p_T selection. The gray dotted contour lines give the LSP mass, $M_{\tilde{e}_R}$, in GeV, as indicated by the labels.

event selection, the number of passed events is compared with the D0 results as described above. We make this comparison for all event selection steps once the third lepton is required, i.e., for step IV and beyond, cf. Table III.

In the following figures, the patterned gray regions mark parameter points with either a neutralino or stau LSP (as indicated in the figures) which are not considered here. The solid gray region exhibits a LSP mass of $M_{\tilde{e}_R} \lesssim 136$ GeV and is thus excluded by the bound on the λ_{231} coupling; cf. Table I. The mass of the $\tilde{e}_R$ LSP (in GeV) is given by the gray contour lines.

In Fig. 2, we give the parameter region that is excluded at 90% C.L. with 2.3 fb^{-1} of analyzed data. We discuss each channel and p_T selection separately. Figure 2(a) [Fig. 2(b)] shows the low-p_T [high-p_T] selection of the $ee\ell$ and $e\mu\ell$ channel. The $\mu\mu\ell$ channel does not exclude any $\tilde{e}_R$ LSP parameter space.

The LSP decays to 50% to a (hard) muon and a neutrino. Thus, the $e\mu\ell$ selection is very sensitive to these models and can exclude $\tilde{e}_R$ LSP scenarios with $\tilde{e}_R$ masses up to 150 GeV (155 GeV) and squark masses up to 850 GeV (880 GeV) with the low-p_T (high-p_T) selection.[12] The sensitivity decreases for lower mass differences of the $\tilde{\chi}_1^0$ and the $\tilde{e}_R$ due to the softer electrons, as can be seen in all displayed channels in Figs. 2(a) and 2(b). Especially the $ee\ell$ channel becomes insensitive in this boundary region.

Comparing the excluded $\tilde{e}_R$ parameter region in Fig. 2 with Fig. 1, we conclude that $\tilde{e}_R$ LSP scenarios with a significant contribution to the anomalous magnetic moment of the muon (region to the left of the green line in Fig. 1) are excluded at 90% C.L. by the D0 search with 2.3 fb^{-1} of analyzed data.[13]

IV. PROSPECTS FOR FUTURE TEVATRON SEARCHES

Both Tevatron experiments D0 and CDF acquired $\sim$10 fb^{-1} of data by the end of 2010. Therefore, we extrapolate the current D0 results to study the prospects of an exclusion of $\tilde{e}_R$ LSP models, using data corresponding to an integrated luminosity of 10 fb^{-1}.

We assume that the events after each selection step in each channel are observed in the same rate as given by

[12]Recall that we only employ the LO cross sections for the signal as a conservative approach. We have explicitly checked with the help of PROSPINO2.1 [56,57] that the NLO signal cross section is always larger than the (fixed) LO one from HERWIG in the relevant regions of parameter space. This statement is also true if we vary the renormalization and factorization scale of the NLO signal cross sections by a factor of 2 and 1/2 around the default central value [56,57]. Therefore, our conclusions are also stable with respect to uncertainties from higher order corrections.

[13]The D0 search rules out all other regions of the B_3 mSUGRA parameter space with a $\tilde{e}_R$ LSP consistent with a_μ (beyond Fig. 1). For $\tan\beta \lesssim 4$, these scenarios are ruled out by the LEP Higgs mass bounds. For $\tan\beta \gtrsim 5.2$, the $\tilde{\tau}_1$ is the LSP. A_0 is strongly constrained by the requirements presented in Ref. [29] and $\mathrm{sgn}(\mu) = -$ is totally ruled out, because SUSY will then give a negative contribution to a_μ [32]. If we go beyond B_3 mSUGRA, then there is still a large parameter region with a $\tilde{e}_R$ LSP allowed [29].

the results with integrated luminosity of 2.3 fb^{-1}; cf. Tables V and VI. Then, we can extrapolate the data to the higher integrated luminosity of 10 fb^{-1}. By applying the same method as in the previous section, we determine the 90% C.L. sensitivity region, i.e., the supersymmetric parameter region which would lead to a significant deviation from the extrapolated data, assuming no discrepancies are observed.

In Fig. 3, we present the $\tilde{e}_R$ LSP parameter space, which can potentially be excluded with a future integrated luminosity of 10 fb^{-1}. The parameter space is the same as in Fig. 2. The 90% C.L. sensitivity regions for the channels $ee\ell$, $e\mu\ell$, and $\mu\mu\ell$ are given by the contour lines for the low-p_T [Fig. 3(a)] and high-p_T [Fig. 3(b)] selection.

The most sensitive channels are the $e\mu\ell$ and $ee\ell$ high-p_T selections, which may exclude scenarios with $M_{1/2} \lesssim 450$ GeV with future data, assuming no deviation from the SM prediction is observed. This corresponds to LSP masses $M_{\tilde{e}_R} \lesssim$ (160–170) GeV and squark masses $M_{\tilde{q}} \lesssim$ (900–950) GeV. As expected, the $e\mu\ell$ selections are more efficient than the $ee\ell$ channels for scenarios with low mass difference between the $\tilde{\chi}_1^0$ and the $\tilde{e}_R$. The $\mu\mu\ell$ channel may become sensitive for models with $M_{1/2} \approx$ (370–380) GeV, because then the $\tilde{t}_1$ decays dominantly via $\tilde{t}_1 \rightarrow \tilde{\chi}_1^+ b$, and the decay of the chargino leads to an enhanced muon multiplicity; cf. Table VIII. However, if the events are observed at the same rate as in the current data, the $\mu\mu\ell$ channel will not play a major role in testing $\tilde{e}_R$ LSP scenarios.

The D0 analysis used in this paper was optimized for associated chargino and neutralino production within R-parity conserving supersymmetry. We point out that larger regions of the selectron LSP parameter space (compared to this paper) can be investigated by the Tevatron collaborations if they optimize their cuts more towards our scenarios. For example, a harder cut on the muon transverse momentum will increase the signal to background ratio. In our models, the muons usually stem from the decay of the (heavy) selectron LSP into two standard model particles and thus have larger momenta. Similarly, a harder cut on $\not{E}_T$ will help, since we have hard neutrinos stemming from the selectron or lightest stau decay and leading to a sizable amount of missing energy [29]. We point out that an *upper* cut on H_T, i.e., the scalar sum of the transverse momenta of all jets, should *not* be applied, because in large regions of the selectron LSP parameter space, sparton-pair production, which leads to hard jets in the final state, occurs at a significant rate.

We conclude this section by pointing out that the D0 analysis is sensitive to an extended $\tilde{e}_R$ LSP parameter space with future data. Under the (strong) assumption that we can linearly extrapolate the results given for an integrated luminosity of 2.3 fb^{-1} to a higher integrated luminosity, $\tilde{e}_R$ LSP scenarios with $M_{1/2} \lesssim 450$ GeV may be probed with 10 fb^{-1}.

V. SUMMARY AND CONCLUSION

A right-handed selectron is a natural candidate for the LSP within the B_3 mSUGRA model. If these or similar models are realized in nature, they usually produce a strong signal of multi charged lepton final states at hadron colliders like the Tevatron. On the one hand, each selectron LSP decay produces one hard charged lepton and missing energy. On the other hand, the decays of heavier SUSY particles into the selectron lead to additional charged leptons.

We have investigated the bounds on these models from the most recent D0 trilepton search (using an integrated luminosity of 2.3 fb^{-1}). The nonobservation of any events beyond the standard model expectation puts stringent bounds on our models. We found that scenarios with selectron LSP (squark) masses of up to 155 GeV (880 GeV) are excluded. We also found that the selectron LSP region consistent with the anomalous magnetic moment of the muon at 2σ (using spectral functions from e^+e^- data) is ruled out by the D0 analysis. Thus, parameter regions outside B_3 mSUGRA should also be considered, for example, nonuniversal scalar masses.

We then extrapolated the D0 trilepton search to larger statistics, i.e., assuming an integrated luminosity of 10 fb^{-1}. If no excess over the standard model expectations is observed, the Tevatron will be able to exclude selectron LSP models with a selectron (squark) mass of up to 170 GeV (950 GeV).

ACKNOWLEDGMENTS

We thank John Conley, Klaus Desch, Sebastian Fleischmann, and Peter Wienemann for helpful discussions. S. G. thanks the Alexander von Humboldt Foundation for financial support. The work of S. G. was also partly financed by the DOE Grant No. DE-FG02-04ER41286. The work of H. K. D. was supported by the BMBF "Verbundprojekt HEP–Theorie" under Contract No. 05H09PDE and the Helmholtz Alliance "Physics at the Terascale."

APPENDIX: SPARTICLE MASSES AND BRANCHING RATIOS OF THE BENCHMARK MODELS

The benchmark scenarios SUSY1 and SUSY2 possess a light sparticle mass spectrum. Therefore, the SUSY contribution to the anomalous magnetic moment of the muon, $\delta a_\mu^{\text{SUSY}}$, agrees within 2σ with the discrepancy between the SM prediction and the observation; cf. Eq. (6). In both benchmark scenarios, SUSY1 and SUSY2, the $\tilde{\tau}_1$ NLSP is nearly mass degenerate with the $\tilde{e}_R$ LSP and exclusively undergoes the R-parity violating decay $\tilde{\tau}_1 \rightarrow e\tilde{\nu}_\mu$. The electrons from this decay usually have a high momentum.

In Table VII, we give the sparticle mass spectrum and the dominant decay modes for SUSY1 [$M_0 = 0$ GeV,

TABLE VII. Branching ratios (BRs) and sparticle masses for the benchmark scenario SUSY1. BRs smaller than 1% are neglected. R-parity violating decays are shown in boldface. Masses which are reduced by more than 5 GeV (compared to the R-parity conserving spectrum) due to $\lambda_{231}|_{\mathrm{GUT}} = 0.045$ are also shown in boldface.

	Mass [GeV]	Channel	BR	Channel	BR
$\tilde{e}_R^-$	**139.1**	$\mu^-\nu_\tau$	**50**%	$\tau^-\nu_\mu$	**50**%
$\tilde{\tau}_1^-$	139.6	$e^-\bar{\nu}_\mu$	**100**%		
$\tilde{\mu}_R^-$	156.2	$\tilde{e}_R^+ e^-\mu^-$	30.2%	$\tilde{e}_R^- e^+\mu^-$	25.1%
		$\tilde{\tau}_1^+\tau^-\mu^-$	24.4%	$\tilde{\tau}_1^-\tau^+\mu^-$	20.3%
$\tilde{\chi}_1^0$	163.3	$\tilde{e}_R^- e^+$	24.7%	$\tilde{e}_R^+ e^-$	24.7%
		$\tilde{\tau}_1^-\tau^+$	22.9%	$\tilde{\tau}_1^+\tau^-$	22.9%
		$\tilde{\mu}_R^-\mu^+$	2.4%	$\tilde{\mu}_R^+\mu^-$	2.4%
$\tilde{\nu}_\tau$	**254.9**	$\tilde{\chi}_1^0\nu_\tau$	63.9%	$W^+\tilde{\tau}_1^-$	24.1%
		$e^-\mu^+$	**12.1**%		
$\tilde{\nu}_\mu$	**258.1**	$\tilde{\chi}_1^0\nu_\mu$	84.5%	$e^-\tau^+$	**15.5**%
$\tilde{\nu}_e$	262.9	$\tilde{\chi}_1^0\nu_e$	100%		
$\tilde{\mu}_L^-$	**269.3**	$\tilde{\chi}_1^0\mu^-$	84.2%	$e^-\bar{\nu}_\tau$	**15.8**%
$\tilde{\tau}_2^-$	**269.6**	$\tilde{\chi}_1^0\tau^-$	63.7%	$H^0\tilde{\tau}_1^-$	13.1%
		$Z^0\tilde{\tau}_1^-$	12.8%	$e^-\bar{\nu}_\mu$	**10.5**%
$\tilde{e}_L^-$	273.9	$\tilde{\chi}_1^0 e^-$	100%		
$\tilde{\chi}_2^0$	311.1	$\tilde{\bar{\nu}}_\tau\nu_\tau$	10.8%	$\tilde{\nu}_\tau\bar{\nu}_\tau$	10.8%
		$\tilde{\bar{\nu}}_\mu\nu_\mu$	9.7%	$\tilde{\nu}_\mu\bar{\nu}_\mu$	9.7%
		$\tilde{\bar{\nu}}_e\nu_e$	8.1%	$\tilde{\nu}_e\bar{\nu}_e$	8.1%
		$\tilde{\mu}_L^-\mu^+$	6.6%	$\tilde{\mu}_L^+\mu^-$	6.6%
		$\tilde{\tau}_2^-\tau^+$	6.3%	$\tilde{\tau}_2^+\tau^-$	6.3%
		$\tilde{e}_L^- e^+$	5.4%	$\tilde{e}_L^+ e^-$	5.4%
		$\tilde{\tau}_1^-\tau^+$	2.7%	$\tilde{\tau}_1^+\tau^-$	2.7%
$\tilde{\chi}_1^-$	311.2	$\tilde{\bar{\nu}}_\tau\tau^-$	22.3%	$\tilde{\bar{\nu}}_\mu\mu^-$	20.0%
		$\tilde{\bar{\nu}}_e e^-$	16.9%	$\tilde{\mu}_L^-\bar{\nu}_\mu$	12.7%
		$\tilde{\tau}_2^-\bar{\nu}_\tau$	12.1%	$\tilde{e}_L^-\bar{\nu}_e$	10.3%
		$\tilde{\tau}_1^-\bar{\nu}_\tau$	5.0%		
$\tilde{t}_1$	365.8	$\tilde{\chi}_1^0 t$	69.1%	$\tilde{\chi}_1^+ b$	30.9%
$\tilde{b}_1$	706.3	$W^-\tilde{t}_1$	78.5%	$\tilde{\chi}_1^- t$	12.8%
		$\tilde{\chi}_2^0 b$	8.2%		
$\tilde{t}_2$	790.6	$Z^0\tilde{t}_1$	55.3%	$H^0\tilde{t}_1$	22.9%
		$\tilde{\chi}_1^+ b$	14.3%	$\tilde{\chi}_2^0 t$	1.2%
$\tilde{\chi}_3^0$	819.8	$\tilde{t}_1\bar{t}$	26.5%	$\tilde{t}_1^* t$	26.5%
		$\tilde{\chi}_1^- W^+$	14.2%	$\tilde{\chi}_1^+ W^-$	14.2%
		$\tilde{\chi}_2^0 Z^0$	12.6%	$\tilde{\chi}_1^0 Z^0$	3.7%
		$\tilde{\chi}_2^0 H^0$	1.0%		
$\tilde{b}_2$	821.5	$\tilde{\chi}_1^0 b$	59.3%	$W^-\tilde{t}_1$	36.8%
		$\tilde{\chi}_1^- t$	2.0%	$\tilde{\chi}_2^0 b$	1.2%
$\tilde{d}_R(\tilde{s}_R)$	824.2	$\tilde{\chi}_1^0 d(s)$	100%		
$\tilde{u}_R(\tilde{c}_R)$	826.3	$\tilde{\chi}_1^0 u(c)$	100%		
$\tilde{\chi}_2^-$	828.0	$\tilde{t}_1^* b$	57.5%	$\tilde{\chi}_2^0 W^-$	12.9%
		$\tilde{\chi}_1^- Z^0$	12.4%	$\tilde{\chi}_1^- H^0$	11.6%
		$\tilde{\chi}_1^0 W^-$	3.3%		
$\tilde{\chi}_4^0$	828.3	$\tilde{t}_1\bar{t}$	34.7%	$\tilde{t}_1^* t$	34.7%
		$\tilde{\chi}_1^- W^+$	9.0%	$\tilde{\chi}_1^+ W^-$	9.0%
		$\tilde{\chi}_2^0 H^0$	7.5%	$\tilde{\chi}_1^0 H^0$	2.2%
$\tilde{u}_L(\tilde{c}_L)$	856.3	$\tilde{\chi}_1^+ d(s)$	65.9%	$\tilde{\chi}_2^0 u(c)$	32.9%
		$\tilde{\chi}_1^0 u(c)$	1.2%		
$\tilde{d}_L(\tilde{s}_L)$	859.8	$\tilde{\chi}_1^- u(c)$	65.5%	$\tilde{\chi}_2^0 d(s)$	32.8%
		$\tilde{\chi}_1^0 d(s)$	1.7%		
$\tilde{g}$	933.8	$\tilde{t}_1\bar{t}$	23.4%	$\tilde{t}_1^* t$	23.4%
		$\tilde{b}_1\bar{b}$	9.2%	$\tilde{b}_1^* b$	9.2%
		$\tilde{b}_2\bar{b}$	2.6%	$\tilde{b}_2^* b$	2.6%
		$\tilde{d}_R\bar{d}(\tilde{s}_R\bar{s})$	2.5%	$\tilde{d}_R^* d(\tilde{s}_R^* s)$	2.5%
		$\tilde{u}_R\bar{u}(\tilde{c}_R\bar{c})$	2.4%	$\tilde{u}_R^* u(\tilde{c}_R^* c)$	2.4%
		$\tilde{u}_L\bar{u}(\tilde{c}_L\bar{c})$	1.3%	$\tilde{u}_L^* u(\tilde{c}_L^* c)$	1.3%
		$\tilde{d}_L\bar{d}(\tilde{s}_L\bar{s})$	1.2%	$\tilde{d}_L^* d(\tilde{s}_L^* s)$	1.2%

TABLE VIII. Same as Table VII, but for the benchmark point SUSY2.

	mass [GeV]	Channel	BR	Channel	BR
$\tilde{e}_R^-$	**151.5**	$\mu^-\nu_\tau$	**50**%	$\tau^-\nu_\mu$	**50**%
$\tilde{\tau}_1^-$	151.6	$e^-\bar{\nu}_\mu$	**100**%		
$\tilde{\chi}_1^0$	152.8	$\tilde{e}_R^- e^+$	50%%	$\tilde{e}_R^+ e^-$	50%
$\tilde{\mu}_R^-$	167.3	$\tilde{\chi}_1^0\mu^-$	100%		
$\tilde{\tau}_\tau$	**250.4**	$\tilde{\chi}_1^0\nu_\tau$	75.7%	$e^-\mu^+$	**12.6**%
		$W^+\tilde{\tau}_1^-$	11.7%		
$\tilde{\nu}_\mu$	**253.7**	$\tilde{\chi}_1^0\nu_\mu$	86.1%	$e^-\tau^+$	**13.9**%
$\tilde{\nu}_e$	258.5	$\tilde{\chi}_1^0\nu_e$	100%		
$\tilde{\mu}_L^-$	**265.0**	$\tilde{\chi}_1^0\mu^-$	85.5%	$e^-\bar{\nu}_\tau$	**14.5**%
$\tilde{\tau}_2^-$	**265.6**	$\tilde{\chi}_1^0\tau^-$	80.6%	$e^-\bar{\nu}_\mu$	**11.6**%
		$Z^0\tilde{\tau}_1^-$	7.7%		
$\tilde{e}_L^-$	269.6	$\tilde{\chi}_1^0 e^-$	100%		
$\tilde{\chi}_2^0$	291.0	$\tilde{\bar{\nu}}_\tau\nu_\tau$	12.0%	$\tilde{\nu}_\tau\bar{\nu}_\tau$	12.0%
		$\tilde{\bar{\nu}}_\mu\nu_\mu$	10.3%	$\tilde{\nu}_\mu\bar{\nu}_\mu$	10.3%
		$\tilde{\bar{\nu}}_e\nu_e$	7.9%	$\tilde{\nu}_e\bar{\nu}_e$	7.9%
		$\tilde{\mu}_L^-\mu^+$	5.5%	$\tilde{\mu}_L^+\mu^-$	5.5%
		$\tilde{\tau}_2^-\tau^+$	5.0%	$\tilde{\tau}_2^+\tau^-$	5.0%
		$\tilde{\tau}_1^-\tau^+$	4.7%	$\tilde{\tau}_1^+\tau^-$	4.7%
		$\tilde{e}_L^- e^+$	3.8%	$\tilde{e}_L^+ e^-$	3.8%
		$\tilde{\chi}_1^0 H^0$	1.0%		
$\tilde{\chi}_1^-$	291.0	$\tilde{\bar{\nu}}_\tau\tau^-$	24.8%	$\tilde{\bar{\nu}}_\mu\mu^-$	21.3%
		$\tilde{\bar{\nu}}_e e^-$	16.4%	$\tilde{\mu}_L^-\bar{\nu}_\mu$	10.5%
		$\tilde{\tau}_2^-\bar{\nu}_\tau$	9.6%	$\tilde{\tau}_1^-\bar{\nu}_\tau$	8.9%
		$\tilde{e}_L^-\bar{\nu}_e$	7.2%	$\tilde{\chi}_1^0 W^-$	1.0%
$\tilde{t}_1$	304.9	$\tilde{\chi}_1^+ b$	100%		
$\tilde{b}_1$	661.6	$W^-\tilde{t}_1$	80.9%	$\tilde{\chi}_1^- t$	11.2%
		$\tilde{\chi}_2^0 b$	7.5%		
$\tilde{t}_2$	750.2	$Z^0\tilde{t}_1$	57.1%	$H^0\tilde{t}_1$	22.2%
		$\tilde{\chi}_1^+ b$	13.2%	$\tilde{\chi}_2^0 t$	5.4%
		$\tilde{\chi}_1^0 t$	1.2%		
$\tilde{b}_2$	779.1	$\tilde{\chi}_1^0 b$	56.7%	$W^-\tilde{t}_1$	39.3%
		$\tilde{\chi}_1^- t$	1.9%	$\tilde{\chi}_2^0 b$	1.2%
$\tilde{d}_R(\tilde{s}_R)$	781.9	$\tilde{\chi}_1^0 d(s)$	100%		
$\tilde{u}_R(\tilde{c}_R)$	783.7	$\tilde{\chi}_1^0 u(c)$	100%		
$\tilde{\chi}_3^0$	793.9	$\tilde{t}_1\bar{t}$	28.5%	$\tilde{t}_1^* t$	28.5%
		$\tilde{\chi}_1^- W^+$	13.0%	$\tilde{\chi}_1^+ W^-$	13.0%
		$\tilde{\chi}_2^0 Z^0$	11.4%	$\tilde{\chi}_1^0 Z^0$	3.3%
		$\tilde{\chi}_2^0 H^0$	1.0%		
$\tilde{\chi}_2^-$	802.1	$\tilde{t}_1^* b$	60.4%	$\tilde{\chi}_2^0 W^-$	11.9%
		$\tilde{\chi}_1^- Z^0$	11.5%	$\tilde{\chi}_1^- H^0$	10.7%
		$\tilde{\chi}_1^0 W^-$	3.0%		
$\tilde{\chi}_4^0$	802.4	$\tilde{t}_1\bar{t}$	36.1%	$\tilde{t}_1^* t$	36.1%
		$\tilde{\chi}_1^- W^+$	8.2%	$\tilde{\chi}_1^+ W^-$	8.2%
		$\tilde{\chi}_2^0 H^0$	6.7%	$\tilde{\chi}_1^0 H^0$	2.0%
$\tilde{u}_L(\tilde{c}_L)$	811.4	$\tilde{\chi}_1^+ d(s)$	66.0%	$\tilde{\chi}_2^0 u(c)$	33.0%
		$\tilde{\chi}_1^0 u(c)$	1.0%		
$\tilde{d}_L(\tilde{s}_L)$	815.0	$\tilde{\chi}_1^- u(c)$	65.5%	$\tilde{\chi}_2^0 d(s)$	32.8%
		$\tilde{\chi}_1^0 d(s)$	1.7%		
$\tilde{g}$	881.0	$\tilde{t}_1\bar{t}$	24.7%	$\tilde{t}_1^* t$	24.7%
		$\tilde{b}_1\bar{b}$	9.5%	$\tilde{b}_1^* b$	9.5%
		$\tilde{b}_2\bar{b}$	2.4%	$\tilde{b}_2^* b$	2.4%
		$\tilde{d}_R\bar{d}(\tilde{s}_R\bar{s})$	2.3%	$\tilde{d}_R^* d(\tilde{s}_R^* s)$	2.3%
		$\tilde{u}_R\bar{u}(\tilde{c}_R\bar{c})$	2.2%	$\tilde{u}_R^* u(\tilde{c}_R^* c)$	2.2%
		$\tilde{u}_L\bar{u}(\tilde{c}_L\bar{c})$	1.2%	$\tilde{u}_L^* u(\tilde{c}_L^* c)$	1.2%
		$\tilde{d}_L\bar{d}(\tilde{s}_L\bar{s})$	1.1%	$\tilde{d}_L^* d(\tilde{s}_L^* s)$	1.1%

$M_{1/2}=400\,\mathrm{GeV}$, $A_0=-1250\,\mathrm{GeV}$, $\tan\beta=5$, $\mathrm{sgn}(\mu)=+$, $\lambda_{231}|_{\mathrm{GUT}}=0.045$]. The $\tilde{e}_R$ LSP mass is about 139 GeV. Because of the low M_0 value, the mass difference between the $\tilde{\chi}_1^0$ next-to-NNLSP and the $\tilde{e}_R$ LSP is about 24 GeV and thus fairly large. The right-handed smuon, $\tilde{\mu}_R$, is the NNLSP and undergoes three-body decays into the $\tilde{e}_R$ LSP and $\tilde{\tau}_1$ NLSP. These decays are discussed in detail in Ref. [29] and usually yield a low-p_T muon. The lightest stop, $\tilde{t}_1$, has a mass of 366 GeV and decays preferably into the $\tilde{\chi}_1^0$ and a t quark. The first and second generation squarks have masses around 820–860 GeV and the gluino mass is 934 GeV.

The sparticle mass spectrum and branching ratios of SUSY2 ($M_0=80$ GeV, $M_{1/2}=375$ GeV, $A_0=-1250$ GeV, $\tan\beta=5$, $\mathrm{sgn}(\mu)=+$, $\lambda_{231}|_{\mathrm{GUT}}=0.045$) are given in Table VIII. This scenario lies near the $\tilde{\chi}_1^0$ LSP region and thus the $\tilde{\chi}_1^0$ NNLSP, the $\tilde{\tau}_1$ NLSP, and the $\tilde{e}_R$ LSP have nearly degenerate masses around 152 GeV. We have a fairly light $\tilde{t}_1$ with a mass of 305 GeV. The $\tilde{t}_1$ decay into the $\tilde{\chi}_1^0$ and a t quark is kinematically forbidden and $\tilde{t}_1\rightarrow\tilde{\chi}_1^+ b$ is the only decay mode. The squarks of the first and second generation have masses around 780–820 GeV and the mass of the gluino is 881 GeV.

[1] H. P. Nilles, Phys. Rep. **110**, 1 (1984).
[2] H. E. Haber and G. L. Kane, Phys. Rep. **117**, 75 (1985).
[3] V. Khachatryan *et al.* (CMS Collaboration), Phys. Lett. B **698**, 196 (2011).
[4] ATLAS Collaboration, Phys. Rev. Lett. **106**, 131802 (2011).
[5] ATLAS Collaboration, arXiv:1102.5290.
[6] CMS Collaboration, Phys. Rev. Lett. **106**, 211802 (2011).
[7] CMS Collaboration, arXiv:1103.1348.
[8] V. M. Abazov *et al.* (D0 Collaboration), Phys. Lett. B **680**, 34 (2009).
[9] T. Aaltonen *et al.* (CDF Collaboration), Phys. Rev. Lett. **101**, 251801 (2008).
[10] R. Forrest (CDF Collaboration), Proceedings of DPF-2009, Detroit, MI, July 2009 (to be published).
[11] H. Baer, K. Hagiwara, and X. Tata, Phys. Rev. Lett. **57**, 294 (1986).
[12] H. Baer, K. Hagiwara, and X. Tata, Phys. Rev. D **35**, 1598 (1987).
[13] V. D. Barger and C. Kao, Phys. Rev. D **60**, 115015 (1999).
[14] K. T. Matchev and D. M. Pierce, Phys. Rev. D **60**, 075004 (1999).
[15] H. Baer, M. Drees, F. Paige, P. Quintana, and X. Tata, Phys. Rev. D **61**, 095007 (2000).
[16] A. Dedes, H. K. Dreiner, U. Nierste, and P. Richardson, arXiv:hep-ph/0207026.
[17] B. C. Allanach, A. Dedes, and H. K. Dreiner, Phys. Rev. D **69**, 115002 (2004).
[18] B. C. Allanach *et al.*, Phys. Rev. D **75**, 035002 (2007).
[19] H. K. Dreiner *et al.*, Nucl. Phys. **B795**, 172 (2008); L. E. Ibanez and G. G. Ross, Nucl. Phys. **B368**, 3 (1992); T. Banks and M. Dine, Phys. Rev. D **45**, 1424 (1992).
[20] H. K. Dreiner, arXiv:hep-ph/9707435.
[21] B. C. Allanach and C. H. Kom, J. High Energy Phys. 04 (2008) 081.
[22] H. K. Dreiner, M. Hanussek, and S. Grab, Phys. Rev. D **82**, 055027 (2010).
[23] B. C. Allanach, A. Dedes, and H. K. Dreiner, Phys. Rev. D **60**, 056002 (1999).
[24] H. K. Dreiner, S. Grab, and M. K. Trenkel, Phys. Rev. D **79**, 016002 (2009); **79**, 019902 (2009).
[25] B. de Carlos and P. L. White, Phys. Rev. D **54**, 3427 (1996).
[26] J. R. Ellis, J. S. Hagelin, D. V. Nanopoulos, K. A. Olive, and M. Srednicki, Nucl. Phys. **B238**, 453 (1984).
[27] M. A. Bernhardt, S. P. Das, H. K. Dreiner, and S. Grab, Phys. Rev. D **79**, 035003 (2009).
[28] H. K. Dreiner and S. Grab, Phys. Lett. B **679**, 45 (2009).
[29] H. K. Dreiner, S. Grab, and T. Stefaniak, arXiv:1102.3189.
[30] Y. Kao and T. Takeuchi, arXiv:0910.4980.
[31] B. Malaescu, arXiv:1006.4739.
[32] D. Stockinger, arXiv:0710.2429.
[33] The Heavy Flavor Averaging Group *et al.*, arXiv:1010.1589.
[34] M. J. Morello (CDF and D0 Collaboration), Proc. Sci., BEAUTY2009 (2009) 048; CDF Collaboration, Public Note Report No. 9892.
[35] S. Schael *et al.* (ALEPH Collaboration, DELPHI Collaboration, L3 Collaboration, OPAL Collaboration, LEP Working Group for Higgs Boson Searches), Eur. Phys. J. C **47**, 547 (2006).
[36] S. Heinemeyer, W. Hollik, and G. Weiglein, Comput. Phys. Commun. **124**, 76 (2000); S. Heinemeyer, W. Hollik, and G. Weiglein, Eur. Phys. J. C **9**, 343 (1999); G. Degrassi, S. Heinemeyer, W. Hollik, P. Slavich, and G. Weiglein, Eur. Phys. J. C **28**, 133 (2003); M. Frank, T. Hahn, S. Heinemeyer, W. Hollik, H. Rzehak, and G. Weiglein, J. High Energy Phys. 02 (2007) 047.
[37] P. Bechtle, O. Brein, S. Heinemeyer, G. Weiglein, and K. E. Williams, Comput. Phys. Commun. **181**, 138 (2010); P. Bechtle, O. Brein, S. Heinemeyer, G. Weiglein, and K. E. Williams, arXiv:1102.1898.
[38] B. C. Allanach, Comput. Phys. Commun. **143**, 305 (2002).
[39] B. C. Allanach and M. A. Bernhardt, Comput. Phys. Commun. **181**, 232 (2010).
[40] G. Belanger, F. Boudjema, A. Pukhov, and A. Semenov, Comput. Phys. Commun. **180**, 747 (2009).
[41] A. Abulencia *et al.* (CDF Collaboration), Phys. Rev. Lett. **98**, 221803 (2007).
[42] T. Aaltonen *et al.* (CDF Collaboration), Phys. Rev. Lett. **99**, 191806 (2007).

[43] V. M. Abazov *et al.* (D0 Collaboration), Phys. Lett. B **638**, 441 (2006).
[44] V. M. Abazov *et al.* (D0 Collaboration), Phys. Rev. Lett. **97**, 111801 (2006).
[45] W. Beenakker, M. Klasen, M. Krämer, T. Plehn, M. Spira, and P. M. Zerwas, Phys. Rev. Lett. **83**, 3780 (1999); **100**, 029901(E) (2008).
[46] M. Cacciari and G. P. Salam, Phys. Lett. B **641**, 57 (2006).
[47] M. Cacciari, G. P. Salam, and G. Soyez, http://www.lpthe.jussieu.fr/~salam/fastjet/.
[48] G. J. Feldman and R. D. Cousins, Phys. Rev. D **57**, 3873 (1998).
[49] Rene Brun and Fons Rademakers, *Proceedings AIHENP'96 Workshop, Lausanne, 1996*; Nucl. Instrum. Methods Phys. Res., Sect. A **389**, 81 (1997); see also http://root.cern.ch/.
[50] F. E. Paige, S. D. Protopopescu, H. Baer, and X. Tata, arXiv:hep-ph/0312045.
[51] G. Corcella *et al.*, J. High Energy Phys. 01 (2001) 010.
[52] G. Corcella *et al.*, arXiv:hep-ph/0210213.
[53] S. Moretti, K. Odagiri, P. Richardson, M. H. Seymour, and B. R. Webber, J. High Energy Phys. 04 (2002) 028.
[54] W. Beenakker, R. Hopker, M. Spira, and P. M. Zerwas, Nucl. Phys. **B492**, 51 (1997); W. Beenakker, M. Krämer, T. Plehn, M. Spira, and P. M. Zerwas, Nucl. Phys. B515, 3 (1998); W. Beenakker, S. Brensing, M. Krämer, A. Kulesza, E. Laenen, and I. Niessen, J. High Energy Phys. 08 (2010) 098; S. Bornhauser, M. Drees, H. K. Dreiner, and J. S. Kim, Phys. Rev. D **76**, 095020 (2007); W. Hollik, M. Kollar, and M. K. Trenkel, J. High Energy Phys. 02 (2008) 018; W. Hollik, E. Mirabella, and M. K. Trenkel, J. High Energy Phys. 02 (2009) 002; H. K. Dreiner, S. Grab, M. Krämer, and M. K. Trenkel, Phys. Rev. D **75**, 035003 (2007).
[55] B. Mele, P. Nason, and G. Ridolfi, Nucl. Phys. **B357**, 409 (1991); S. Frixione, P. Nason, and G. Ridolfi, Nucl. Phys. **B383**, 3 (1992); J. Ohnemus, Phys. Rev. D **44**, 1403 (1991); M. Cacciari, S. Frixione, M. L. Mangano, P. Nason, and G. Ridolfi, J. High Energy Phys. 04 (2004) 068; R. Bonciani, S. Catani, M. L. Mangano, and P. Nason, Nucl. Phys. **B529**, 424 (1998); **B803**, 234 (2008); J. M. Campbell, F. Maltoni, and F. Tramontano, Phys. Rev. Lett. **98**, 252002 (2007); J. M. Campbell and R. K. Ellis, Phys. Rev. D **65**, 113007 (2002); G. Altarelli, R. K. Ellis, and G. Martinelli, Nucl. Phys. **B157**, 461 (1979).
[56] W. Beenakker, R. Hopker, and M. Spira, arXiv:hep-ph/9611232.
[57] www.thphys.uni-heidelberg.de/~plehn/prospino.